Louisiana State University

LSU Digital Commons

1-1-2001

Cure for unstable numerical evolutions of single black holes: Adjusting the standard ADM equations in the spherically symmetric case

Bernard Kelly
Pennsylvania State University

Pablo Laguna
Pennsylvania State University

Keith Lockitch
Pennsylvania State University

Jorge Pullin
Pennsylvania State University

Erik Schnetter
Pennsylvania State University

See next page for additional authors

Recommended Citation

Authors

Bernard Kelly, Pablo Laguna, Keith Lockitch, Jorge Pullin, Erik Schnetter, Deirdre Shoemaker, and Manuel Tiglio

A cure for unstable numerical evolutions of single black holes: adjusting the standard ADM equations

Bernard Kelly, Pablo Laguna, Keith Lockitch, Jorge Pullin, Erik Schnetter, Deirdre Shoemaker and Manuel Tiglio

Center for Gravitational Physics & Geometry,

Penn State University, University Park, PA 16802

Numerical codes based on a direct implementation of the standard ADM formulation of Einstein's equations have generally failed to provide long-term stable and convergent evolutions of black hole spacetimes when excision is used to remove the singularities. We show that, for the case of a single black hole in spherical symmetry, it is possible to circumvent these problems by adding to the evolution equations terms involving the constraints, thus adjusting the standard ADM system. We investigate the effect that the choice of the lapse and shift has on the stability properties of numerical simulations and thus on the form of the added constraint term. To facilitate this task, we introduce the concept of quasi well-posedness, a version of well-posedness suitable for ADM-like systems involving second-order spatial derivatives.

I. INTRODUCTION

In numerical relativity, Einstein's equations are usually solved as an initial value problem. That is, the spacetime is foliated with spacelike hypersurfaces. These hypersurfaces, or slices, are characterized by their intrinsic geometry (spatial metric g_{ij}) and extrinsic curvature K_{ij}. Subsequent slices in a given foliation are connected via the lapse function α and shift vector β^i [1]. Under this framework, the components of Einstein's equation naturally separate into constraint and evolution equations for the dynamical variables g_{ij} and K_{ij}. Thus, a typical procedure to construct a spacetime consists of first specifying Cauchy data (g_{ij}, K_{ij}) that satisfy the constraints on the initial slice and then applying the evolution equations to update these data into the next slice. This procedure is known as free or unconstrained evolution.

In order to propagate (g_{ij}, K_{ij}) using the evolution equations, one must provide in addition a prescription for choosing the lapse function and shift vector. One generally regards the lapse-shift prescription as a choice of coordinates. At the continuum level, given a lapse-shift choice and a specific set of Cauchy data, the evolution equations yield not only a unique spacetime metric expressed in a given coordinate system but also evolved data (g_{ij}, K_{ij}) that continues to satisfy the constraints.

Numerical approximations are likely to complicate the picture described above. For instance, because of truncation errors, the data (g_{ij}, K_{ij}) do not satisfy the continuum Einstein constraints but rather their discrete approximations. Even if consistency between the numerical approximations of the evolution and constraint equations is achieved, the evolved data (g_{ij}, K_{ij}) will at best satisfy the constraints up to truncation errors. Of course, this is what one should expect. However, the presence of numerical errors could also trigger fast growing modes that render the numerical evolution unstable. Characterizing and controlling these growing modes has been and continues to be one of the most difficult and demanding tasks in numerical relativity.

The origin of these destabilizing modes is multiple. Unstable modes could be purely numerical (e.g., the Courant instability) or they could be present already at the continuum level. An example of continuum instabilities are the so called constraint-violating modes [2]. These are solutions of the Einstein evolution equations that do not satisfy the Hamiltonian and momentum constraints. The general perception is that this class of solutions consists mostly of rapidly growing solutions, although there is no formal proof that this is indeed the case. In summary, even if one were to start an evolution with "perfect" initial data that satisfies the constraints, truncation errors could cause the numerical solution to drift into a constraint-violating, and perhaps unbound, solution.

Various groups have accumulated numerical evidence supporting as a possible cause of instabilities the particular 3+1 form used to recast Einstein's equation as an initial value problem. These observations have partially motivated the development of hyperbolic formulations of Einstein equations [3–8]. Hyperbolic formulations have the advantage that mathematical tools exist to prove existence and uniqueness of the solutions as well as well-posedness, thus providing important information for the implementation of stable discretization algorithms. If excision is used to handle the singularities, numerical simulations of black hole spacetimes require the imposition not only of outgoing, radiative boundary conditions far away from the holes but also of conditions on the excision boundary that respect the propagation of physical modes to flow down into the hole. Because hyperbolic formulations also yield information regarding the characteristics of all the field variables in the system, in principle this knowledge could be extremely useful when applying these boundary conditions.

Unfortunately, so far, none of the numerical efforts based on hyperbolic formulations of Einstein equations have been able to demonstrate their clear superiority. Currently, the formulation originally developed by Shibata and Nakamura [9], and later re-introduced by Baugarte and Shapiro [10], (BSSN) seems to be the least prone to instabilities. Interestingly enough, the BSSN formulation is not explicitly hyperbolic. Just recently, a numerical implementation of the Einstein-Christoffel hyperbolic system [7] has been applied to single black hole spacetime and produced three-dimensional evolutions with stability properties comparable to those using the BSSN formulation [11]. The common lore these days is, however, that the standard Arnowitt-Deser-Misner (ADM) [12] formulation is the one which most easily suffers from instabilities [13–15]. On the other hand, the ADM formulation has the advantage of containing a minimal number of equations, making it attractive for numerical studies.

The main objective of this paper is to show that, given a choice of lapse function and shift vector, it is possible to obtain long-term stable and convergent simulations using the standard ADM formulation if "appropriate" terms involving the constraints are added to the evolution equations. Of course, here the key ingredient is to understand what constitutes an appropriate choice of constraint terms. We show that at least in spherical symmetry, it is possible to obtain a definite prescription for adding these constraint-terms that only depends on the choice of gauge or coordinate conditions, namely the lapse and shift. The idea of adding constraint-terms to the evolution equations (adjusted ADM formulations) is not new [16]. Just recently, Yoneda and Shinkai [17] studied in full detail the propagation of the constraints in the family of adjusted ADM systems.

In order to help identify what constitutes a suitable choice of constraint-terms, we introduce a definition of quasi well-posedness. The idea of quasi well-posedness is simply to make choices of lapse and shift such that, when the ADM system is enlarged with the addition of new variables (typically, but not always, quantities related to the first spatial derivatives of the three metric), one obtains a strongly hyperbolic system. Once a strongly hyperbolic system is obtained, one can make use of the standard results that apply to those systems regarding the existence, uniqueness and well-posedness of the solutions. The essence of quasi well-posedness is then that the properties of the strongly hyperbolic system are to some degree inherited by the original ADM system. The advantage of this procedure is that by looking at the strongly hyperbolic system, one is also able to gain insight about the propagation of the constraints and characteristics of the original system, thus improving the chances of obtaining stable numerical evolutions.

In Sec. II, we introduce the concept of quasi well-posedness. The explicit form of the equations and initial data used in our numerical evolutions are described in Sec. III. The prescription to adjust the standard ADM equations is presented in Sec. IV. We investigate in Sec. V the implications of the presence of gauge modes. Next, in Sec. VI, we discuss the quasi well-posedness properties of the adjusted ADM system under three lapse and shift conditions. For each of these conditions, we present numerical results showing the stability properties of the simulations. We end in Sec. VII with concluding remarks.

II. QUASI WELL-POSEDNESS

To understand the general idea of quasi well-posedness, let us consider the initial value problem for the wave equation $\partial_{tt}\,\varphi = \partial_{xx}\,\varphi$, ignoring boundaries. By adding a new variable, $\pi = \partial_t\,\varphi$, this equation takes the form

$$\partial_t\,u = P\,\partial_{xx}\,u + Qu\,,\tag{2.1}$$

where

$$u = \begin{pmatrix} \varphi \\ \pi \end{pmatrix}\,, \quad P = \begin{pmatrix} 0 & 0 \\ 1 & 0 \end{pmatrix} \quad \text{and} \quad Q = \begin{pmatrix} 0 & 1 \\ 0 & 0 \end{pmatrix}\,.$$

One can view the system of equations (2.1) as the analogue of the standard ADM equations. Now, adding one more variable, $\xi = \partial_x\,\varphi$, we rewrite (2.1) as a first order system in both time and space. That is,

$$\partial_t\,\tilde{u} = A\,\partial_x\,\tilde{u} + B\tilde{u}\,,\tag{2.2}$$

with

$$\tilde{u} = \begin{pmatrix} \varphi \\ \pi \\ \xi \end{pmatrix}\,, \quad A = \begin{pmatrix} 0 & 0 & 0 \\ 0 & 0 & 1 \\ 0 & 1 & 0 \end{pmatrix} \quad \text{and} \quad B = \begin{pmatrix} 0 & 1 & 0 \\ 0 & 0 & 0 \\ 0 & 0 & 0 \end{pmatrix}\,.$$

Notice that one needs to supplement the system (2.2) with the the constraint $C = \xi - \partial_x\,\varphi$. For this simple case, one can find estimates for the solution u from (2.1) directly, but the idea here is not to do so but rather to use what is known about the first order system (2.2). The matrix A has the following set of eigenvalues and eigenvectors:

2

$$\begin{aligned}
\lambda_1 &= 1 && \text{with eigenvector} && \vec{e}_1 = [0,1,1] \\
\lambda_2 &= 0 && \text{with eigenvector} && \vec{e}_2 = [1,0,0] \\
\lambda_3 &= -1 && \text{with eigenvector} && \vec{e}_3 = [0,-1,1] \,.
\end{aligned} \tag{2.3}$$

Given that the matrix A has real eigenvalues and a complete system of eigenvectors, the system of equations (2.2) is strongly hyperbolic [1] and thus well-posed. In this case, the matrix A is also Hermitian (symmetric hyperbolicity). and has real and distinct eigenvalues (strictly hyperbolic)

Since the system (2.2) is well-posed, we can establish existence and uniqueness of the solution to (2.2), together with the usual condition:

$$||\tilde{u}(t,\ )||^2 \le D\,e^{a\,t}||\tilde{u}(0,\ )||^2 \,, \tag{2.4}$$

with a and D independent of the initial data and $||\ ||$ the L_2 norm. Furthermore, because the vector $\tilde{u}$ contains u as part of its components,

$$||u(t,\ )||^2 \le ||\tilde{u}(t,\ )||^2 \,.$$

It follows then from equation (2.4) that the solution of the system (2.1) satisfies the condition

$$||u(t,\ )||^2 \le D\,e^{a\,t}\left(||u(0,\ )||^2 + ||\partial_x\,u(0,\ )||^2\right) \,. \tag{2.5}$$

We should remark that, although (2.5) was derived using L_2 norms, the solution could in general be bounded by the initial data in some other Sobolev norm. The importance of the condition (2.5) and similar bounds is that it guarantees, among other things, that the solutions to (2.1) will not have unbounded high frequency modes. In numerical calculations however, this is not enough. For practical purposes, even large power-law growths such as t^4 are likely to be extremely problematic [2].

The idea is then to investigate quasi well-posedness in the standard ADM formulation. That is, given a choice of lapse and shift, one enlarges the standard ADM system introducing new variables that render the system at least strongly hyperbolic. Existence, uniqueness and well-posedness for the ADM equations will then follow from the corresponding usual properties of the strongly hyperbolic system. In some instances, to obtain such hyperbolic formulations it is not enough just to add the spatial derivatives of the metric as new variables, but one also has to add the constraints to the evolution equations, or even take combinations of these evolution equations. But the general idea is the same: add the constraints and/or take the same combination in the ADM equations as one does in the strongly hyperbolic system. It will be in this sense that we will refer, in what follows, to the quasi well-posedness of some ADM systems.

It is important to mention that for this analysis we have neglected the effects from boundary conditions. For the case under consideration (single black hole evolutions via excision of the singularity) boundary conditions at the excised region do not affect quasi well-posedness since, as we shall see, all the characteristics of the system are outgoing into the hole. At the outer edge of the computational domain, we use the exact analytic solution as boundary condition. Our numerical results show that this does not influence the properties drawn from quasi well-posedness for the class of gauge choices and added constraint-terms we considered.

III. THE $\dot{G} - \dot{K}$ EQUATIONS

Although the idea of quasi well-posedness can be applied to more general systems, throughout this paper we will concentrate on the ADM evolution equations ($\dot{g} - \dot{K}$ equations) obtained from the vanishing of the Ricci tensor, i.e.

$$\partial_t g_{ij} - \mathcal{L}_\beta g_{ij} = -2\,\alpha\,K_{ij} \,, \tag{3.1}$$

$$\partial_t K_{ij} - \mathcal{L}_\beta K_{ij} = -\nabla_i\nabla_j\alpha + \alpha\left(R_{ij} + K\,K_{ij} - 2K_{ik}\,K^k{}_j\right) \tag{3.2}$$

As customary in numerical relativity, we will focus on free evolutions; that is, we will not enforce the constraints

---

[1]Following [18], a system is called symmetric hyperbolic if the matrix A is Hermitian. It is called strictly hyperbolic if the eigenvalues are real and distinct; it is called strongly hyperbolic if the eigenvalues are real and there exists a complete system of eigenvectors; and, finally, it is called weakly hyperbolic if the eigenvalues are real.

$$2\,H \equiv R + K^2 - K_{ij}K^{ij} = 0 \tag{3.3}$$

$$M^i \equiv \nabla_j(K^{ij} - g^{ij}K) = 0\,, \tag{3.4}$$

except at the initial data. Finally, to facilitate our analysis, we will only consider a single black hole in spherical coordinates. The most general time-dependent spherically symmetric metric in a 3+1 form is:

$$ds^2 = (-\alpha^2 + a^2\,\beta^2)\,dt^2 + 2\,a^2\,\beta\,dt\,dr + a^2\,dr^2 + b^2\,d\Omega^2\,, \tag{3.5}$$

where all functions are assumed to depend only on r and t; $d\Omega^2 \equiv d\theta^2 + \sin^2\theta\,d\phi^2$, and $\beta \equiv \beta^r$. In these spherical coordinates, the spatial metric, extrinsic curvature and Ricci tensor are diagonal:

$$g_{ij} = \mathrm{diag}(a^2,\,b^2,\,b^2\,\sin^2\theta) \tag{3.6}$$

$$K^i{}_j = \mathrm{diag}(K_a,\,K_b,\,K_b) \tag{3.7}$$

$$R^i{}_j = \mathrm{diag}(R_a,\,R_b,\,R_b)\,. \tag{3.8}$$

The $\dot{g}$–$\dot{K}$ equations take the form

$$(\partial_t - \beta\,\partial_r)\,a = -\alpha\,a\,K_a + a\,\partial_r\,\beta \tag{3.9}$$

$$(\partial_t - \beta\,\partial_r)\,b = -\alpha\,b\,K_b \tag{3.10}$$

$$(\partial_t - \beta\,\partial_r)\,K_a = -\frac{1}{a^2}\left(\partial_r^2\alpha - \frac{1}{a}\partial_r a\,\partial_r\alpha\right) + \alpha\,[R_a + (K_a + 2\,K_b)\,K_a] \tag{3.11}$$

$$(\partial_t - \beta\,\partial_r)\,K_b = -\frac{1}{b\,a^2}\partial_r b\,\partial_r\alpha + \alpha\,[R_b + (K_a + 2\,K_b)\,K_b]\,, \tag{3.12}$$

and the constraints

$$H \equiv \frac{R_a}{2} + R_b + 2\,K_a\,K_b + K_b^2 = 0 \tag{3.13}$$

$$M \equiv \partial_r K_b + (K_b - K_a)\,\frac{\partial_r b}{b} = 0\,, \tag{3.14}$$

where the components of the Ricci tensor are given by

$$R_a = \frac{2}{a^3\,b}\left(-a\,\partial_r^2 b + \partial_r a\,\partial_r b\right) \tag{3.15}$$

$$R_b = \frac{1}{a^3\,b^2}\left[-b\,a\,\partial_r^2 b + b\,\partial_r a\,\partial_r b + a^3 - a\,(\partial_r b)^2\right]\,. \tag{3.16}$$

Our numerical results consist of free-evolutions of analytic, single black hole initial data $(a,\,b,\,K_a,\,K_b)$ in a computational domain $r_e \leq r \leq r_o$, where r_o denotes the location of the outer boundary far from the hole and r_e the excision boundary inside the black hole horizon. The numerical code used solves the $\dot{g} - \dot{K}$ equations in the interior of the computational domain by the method of lines. That is, the $\dot{g} - \dot{K}$ system has the generic form

$$\partial_t\,u = \beta\,\partial_r\,u + \rho\,, \tag{3.17}$$

with $u = u(a,\,b,\,K_a,\,K_b)$ and ρ given by the r.h.s. of equations (3.9–3.12). The starting point is then to approximate the derivatives appearing in ρ by second order accurate, centered finite differences. On the other hand, the the spatial derivative in the "advection" term $\beta\,\partial_r u$ is approximated by an upwind discretization [19] of the form:

$$\partial_r\,u_i \approx \Delta_r u_i \equiv \frac{(u_{i+1} - u_{i-1})}{2\,\Delta r} \pm q\frac{(u_{i\mp1} - 3\,u_i + 3\,u_{i\pm1} - u_{i\pm2})}{3\,\Delta r} \tag{3.18}$$

where $q \geq 0$ and the choice of sign is given by $\pm = \mathrm{sign}(\beta)$. As we shall later see, for the black hole spacetime metrics under consideration, the shift vector is always non-negative. Thus, the discretization (3.18) is only needed with the upper sign. The above upwind discretization has truncation error:

$$\tau_i \equiv \Delta_r u_i - \partial_r\,u_i = \frac{1}{6}\,(1 - 2\,q)\,\Delta r^2\,\partial_r^3\,u_i \mp \frac{q}{6}\,\Delta r^3\,\partial_r^4 u_i\,. \tag{3.19}$$

Thus, the discretization is second order accurate for any choice of the adjustable parameter q, except for $q = 0.5$ when the truncation errors are of $O(\Delta r^3)$. In our simulations, we set $q = 0.5$. This value yields both stable evolutions and

minimizes the amount of dissipation introduced by the discretization. After the discretization of the spatial differential operators, Eq. (3.17) becomes a set of ordinary differential equations for the interior grid points $\{r_i\}_{i=1,...,N-1}$. The grid values r_0 and r_N denote the locations of the inner and outer boundaries, respectively. The temporal updating of these equations is carried out via an iterated Crank Nicholson method [20]. Notice that at the outer-most grid point r_{N-1}, the upwind scheme (3.18) requires "ghost" values at r_{N+1}. These values are computed using second or third order accurate extrapolations.

Next is the implementation of boundary conditions. As mentioned before, there are two boundaries in the problem, one far from the black hole at $r_N = r_o$ and a second at the point of excision, $r_0 = r_e$. The boundary condition used at r_o is that all field variables take the values provided by the exact analytic solution. It is important to notice that in previous efforts in numerical evolutions of spherically symmetric black hole spacetimes, the stability of the evolutions depended not only in the location of the outer boundary but also on the imposition of "outgoing" boundary conditions. One of these outgoing conditions is constructed by assuming that the solution error $u - \bar{u}$ is of the form $\epsilon(t - r)/r^n$, with $\bar{u}$ the analytic exact solution. This condition yields

$$\partial_t \, u = -\partial_r \, u + \partial_r \, \bar{u} + n \, \frac{(u - \bar{u})}{r} \, , \tag{3.20}$$

to be applied at the nodal grid point $r_N = r_o$ The outgoing condition (3.20) is then added to the system (3.17) and handled with the same method of lines used for the interior points. Obviously, there is no reason to believe that the solution error should behave as $\epsilon(t-r)/r^n$ for general choices of lapse and shift. Another approach to construct outer boundary conditions that has been used is to blend [21] the numerical solution to the analytic one beyond a certain radius, r.

Finally, at the inner or excision boundary, the working assumption is that all of the fields have outgoing (into the hole) characteristics. We will show that for the gauge or coordinate conditions under consideration, this is indeed the situation. Therefore, there is no need to impose any boundary condition, and one can just apply at r_e the same system of equations used in the interior of the computational domain. However, finite difference discretization would require "ghost" values at r_{-1}. We construct these values by extrapolation. Another possibility, which is becoming popular in three-dimensional simulations [22], is instead to extrapolate the r.h.s. of Eq. (3.17) to $r_0 = r_e$. Either approach was stable for the cases considered in the present work.

An important requirement when performing numerical simulations of black holes in which the singularities are excised from the computational domain is to use coordinates that are regular and penetrate the horizon. Foliations that penetrate the horizon facilitate the task of removing (i.e. excising) a region containing the black hole singularity while preserving the causal structure of the spacetime exterior to the event horizon. Thus the numerical results we present here consist of numerical evolutions that for infinite resolution correspond to the solution of a single black hole expressed in ingoing-Eddington-Finkelstein (iEF) and also Painlevé-Gullstrand (PG) [23,24]. coordinates. The iEF coordinates coincide with Kerr-Schild coordinates in the case of zero angular momentum [25]. Recently, Martel and Poisson [26] have showed that the PG and iEF coordinates are members of the same one-parameter family of coordinate systems.

In iEF coordinates, the line element (3.5) takes the explicit form

$$ds^2 = -\left(1 - \frac{2\,m}{r}\right) dt^2 + \frac{4m}{r} dt \, dr + \left(1 + \frac{2\,m}{r}\right) dr^2 + r^2 d\Omega^2 \, . \tag{3.21}$$

The ADM variables in these coordinates are given by:

$$\alpha = \left(1 + \frac{2\,m}{r}\right)^{-1/2} \tag{3.22}$$

$$\beta = \frac{2\,m}{r} \left(1 + \frac{2\,m}{r}\right)^{-1} \tag{3.23}$$

$$a = \left(1 + \frac{2\,m}{r}\right)^{1/2} \tag{3.24}$$

$$b = r \tag{3.25}$$

$$K_a = -\frac{2\,m}{r^3}(r + m) \left(1 + \frac{2\,m}{r}\right)^{-3/2} \tag{3.26}$$

$$K_b = \frac{2\,m}{r^2} \left(1 + \frac{2\,m}{r}\right)^{-1/2} \, . \tag{3.27}$$

Similarly, for PG coordinates

$$ds^2 = -\left(1 - \frac{2\,m}{r}\right)dt^2 + 2\sqrt{\frac{2\,m}{r}}\,dt\,dr + dr^2 + r^2 d\Omega^2 \,, \tag{3.28}$$

and

$$\alpha = 1 \tag{3.29}$$

$$\beta = \sqrt{\frac{2\,m}{r}} \tag{3.30}$$

$$a = 1 \tag{3.31}$$

$$b = r \tag{3.32}$$

$$K_a = -\frac{\beta}{2\,r} \tag{3.33}$$

$$K_b = \frac{\beta}{r}\,. \tag{3.34}$$

The geometrical interpretation of the iEF coordinate system is that in addition to having a timelike killing vector, the combination of timelike and radial tangent vectors $\vec{\partial}_t - \vec{\partial}_r$ remains null. In terms of the spacetime metric, this condition is stated as $g_{tt} - 2\,g_{tr} + g_{rr} = 0$, or similarly in terms of 3+1 metric functions as $\alpha = a\,(1 - \beta)$. On the other hand, the PG coordinate system can be viewed as that anchored to a family of freely moving observers (time-like) starting at infinity with vanishing velocity [26].

Finally, in numerical evolutions of spherically symmetric spacetimes, it is useful to monitor not only the Hamiltonian and momentum constraints but to pay attention also to the mass function

$$\mathcal{M}(r,t) = \frac{b}{2}(1 - \nabla_\mu b\,\nabla^\mu b)\,. \tag{3.35}$$

In vacuum, this $\mathcal{M}$ is the gauge invariant definition of mass.

IV. ADJUSTED ADM SYSTEMS

Each of the equations in the $\dot{g}$–$\dot{K}$ or standard ADM system (3.9-3.12) has the form

$$\partial_t\,u_{(n)} - \beta\,\partial_r\,u_{(n)} = B_{(n)}\,u_{(n)} + C_{(n)} \tag{4.1}$$

(no summation over n) with

$$u_{(n)} = (a,\,b,\,K_a,\,K_b) \tag{4.2}$$

$$B_{(n)} = \text{diag}(-\alpha\,K_a + \partial_r\,\beta,\,-\alpha\,K_b,\,2\,\alpha\,K_b,\,\alpha\,K_a) \tag{4.3}$$

The $C_{(n)}$ contain the remaining terms that cannot be written in the form $B_{(n)}\,u_{(n)}$, with $B_{(n)}$ independent of $u_{(n)}$. If one views each equation as independent, that is β, $B_{(n)}$ and $C_{(n)}$ as given and independent of $u_{(n)}$, Eqs. (4.1) admit rapidly growing solutions if $B_{(n)} > 0$, exponentially growing if $B_{(n)}$ and β are non-negative constants. Obviously, when the equations (4.1) are considered as a coupled system of equations, one cannot guarantee the above conclusion. However, we have been able to track the problems observed in our numerical evolutions to those terms for which $B_{(n)} > 0$.

In iEF and PG coordinates, the second and fourth components of $B_{(n)}$ are non-positive. The first component of $B_{(n)}$ vanishes for PG coordinates and is positive for iEF. Finally, the third component of $B_{(n)}$ is always non-negative, for both iEF and PG coordinates. Our numerical experiments indicate that the origin of the instabilities is due to the term involving $B_{(n=3)} = 2\,\alpha\,K_b$. The term in iEF coordinates involving $B_{(n=1)}$ with the "wrong" sign did not seem to affect the evolutions (see results below).

The objective is then to find a way to "change the sign" of $B_{(n=3)}$. Fortunately, the combination $K_b\,K_a$ also appears in the Hamiltonian constraint (3.13). One can then add to the evolution equation for K_a a term of the form $-\mu\,\alpha\,H$. As a consequence, $B_{(n=3)} = 2\,(1 - \mu)\,\alpha\,K_b$. Therefore, in principle, any value of $\mu \geq 1$ should produce stable evolutions. Our numerical simulations show that $\mu = 2$ is an optimal value to reach quickly the time independent solution. However, the same experiments indicate also that even values of $\mu \approx 0.5$ yield stable evolutions. The reason for this is likely because the simple analysis above does not take into consideration the non-linear coupling in the equations.

6

V. LINEAR GAUGE MODES

A potential source of instabilities in numerical simulations is the presence of gauge modes. Gauge modes arise because a prescription of the lapse and shift is not sufficient for complete gauge fixing. If the lapse and shift functions are for instance determined from algebraic expressions or differential equations, there is still remaining freedom left to perform coordinate transformation that take us from (g_{ij}, K_{ij}) to $(\tilde{g}_{ij}, \tilde{K}_{ij})$, leaving the lapse-shift prescription invariant. In other words, the data (g_{ij}, K_{ij}) will be unique up to coordinate transformations that leave the lapse-shift prescription invariant. One can then encounter the situation in which the transformed pair $(\tilde{g}_{ij}, \tilde{K}_{ij})$ continues to satisfy the constraints, but it possesses unbounded growths. In principle, because $(\tilde{g}_{ij}, \tilde{K}_{ij})$ are allowed solutions to the evolution equations, one could through numerical convergence and monitoring of the constraints single out these modes. In practice the situation is not that simple. Gauge conditions that allow the rapid growth of grid functions are likely to trigger numerical instabilities.

To investigate these modes, let us consider an infinitesimal coordinate transformation,

$$x^\mu \to x^\mu + \xi^\mu \,, \tag{5.1}$$

This transformation induces a linear perturbation of the spacetime metric,

$$g_{\mu\nu} \to g_{\mu\nu} + \delta g_{\mu\nu} \,, \tag{5.2}$$

of the form

$$\delta g_{\mu\nu} = -\mathcal{L}_\xi \, g_{\mu\nu}. \tag{5.3}$$

In spherical symmetry, the most general coordinate transformation is

$$t \to t + \delta t(r, t) \tag{5.4}$$

$$r \to r + \delta r(r, t) \,, \tag{5.5}$$

or equivalently

$$\xi^\mu = (\delta t, \delta r, 0, 0) \,. \tag{5.6}$$

Given (5.6), the gauge induced perturbations of the metric takes the form

$$\delta g_{tt} = -2\left(-\alpha^2 + a^2\beta^2\right)\partial_t \delta t - 2a^2\beta\,\partial_t \delta r - \partial_t\left(-\alpha^2 + a^2\beta^2\right)\delta t - \partial_r\left(-\alpha^2 + a^2\beta^2\right)\delta r \tag{5.7}$$

$$\delta g_{tr} = -a^2\beta\,\partial_t\delta t - a^2\,\partial_t\delta r - \left(-\alpha^2 + a^2\beta^2\right)\partial_r\delta t - a^2\beta\,\partial_r\delta r - \partial_t\left(a^2\beta\right)\delta t - \partial_r\left(a^2\beta\right)\delta r \tag{5.8}$$

$$\delta g_{rr} = -2a^2\beta\,\partial_r\delta t - 2a^2\,\partial_r\delta r - \partial_t\left(a^2\right)\delta t - \partial_r\left(a^2\right)\delta r \tag{5.9}$$

$$\delta g_{\theta\theta} = -\partial_t\left(b^2\right)\delta t - \partial_r\left(b^2\right)\delta r \tag{5.10}$$

$$\delta g_{\phi\phi} = \delta g_{\theta\theta}\,\sin^2\theta \,, \tag{5.11}$$

with all remaining components vanishing. On the other hand, from (3.5), the components of the perturbed metric $\delta g_{\mu\nu}$ above are also given by:

$$\delta g_{tt} = -2\,\alpha\,\delta\alpha + 2\,a\,\delta a\,\beta^2 + 2\,a^2\,\beta\,\delta\beta \tag{5.12}$$

$$\delta g_{tr} = 2\,a\,\delta a\,\beta + a^2\,\delta\beta \tag{5.13}$$

$$\delta g_{rr} = 2\,a\,\delta a \tag{5.14}$$

$$\delta g_{\theta\theta} = 2\,b\,\delta b \,. \tag{5.15}$$

In studying these gauge perturbations, we consider a number of different prescriptions for choosing the lapse and shift. These impose restrictions on the components of $\delta g_{\mu\nu}$ to linear order, but are not sufficient for complete gauge fixing.

One piece of evidence usually given to argue for the highly unstable properties of the standard ADM formulation is its inability to simulate single black hole spacetimes. Specifically, the problem consists of using a known analytic black hole solution of Einstein's equation to construct initial data, set boundary conditions and specify the lapse and shift. Given this input, the output is the numerical evolution of the spatial metric g_{ij} and extrinsic curvature K_{ij}. This simple setup does not yield stable evolutions.

Choosing the lapse and shift to be given by the exact analytic solutions implies that in the coordinate transformations above, $\delta\alpha = \delta\beta = 0$. We shall call this the "exact lapse + exact shift" (EL+ES) condition, It is clear from (5.7–5.11) that the EL+ES choice does not fix the coordinates uniquely, but rather results in a non-trivial system of PDE's to be satisfied by δt and δr. The solutions to this PDE system form an equivalence class of gauges all satisfying the same condition on the lapse and shift. At the analytic level, one selects a unique member of this equivalence class by imposing boundary and initial conditions. Numerically however, because of truncation errors, this is only possible if the evolution is stable.

Substitution of $\delta\alpha = \delta\beta = 0$ in (5.12-5.14) yields $\delta g_{tr} - \beta\,\delta g_{rr} = \delta g_{tt} - \beta^2\,\delta g_{rr} = 0$. Using (5.7–5.9), these conditions can be rewritten in terms of the gauge perturbation ξ^μ as

$$\partial_t\xi = A\partial_r\xi + B\xi \tag{5.16}$$

where

$$\xi = \begin{pmatrix} \delta t \\ \delta r \end{pmatrix} \quad \text{and} \quad A = \begin{pmatrix} \beta & 0 \\ \frac{\alpha^2}{a^2} & \beta \end{pmatrix} .$$

The matrix A has a degenerate eigenvalue $\lambda = \beta$ and corresponding eigenvector $\vec{e} = [0,\,1]$. Therefore, the system is only weakly hyperbolic and thus ill-posed. It is then not possible to guarantee the absence of rapidly growing gauge modes. Gauge instabilities, by themselves, do not violate the constraints; however, they are likely to trigger numerical instabilities and thereby couple to constraint-violating modes. Note that this conclusion does not depend on the use of the standard ADM formulation, but it applies to any initial value formulation of Einstein's equation. This is likely the reason why it has not been possible to produce hyperbolic formulations of Einstein equations using the EL+ES lapse-shift condition. Other groups have reported numerical instabilities associated with an EL+ES prescription. (See, for example, [27,28].) Our result, which provides some analytic insight into the source of these instabilities, extends the analysis of Ref. [27] by including perturbations of a general spherically symmetric spacetime (3.5) and by making no assumptions about the form of the coupling between gauge and constraint-violating perturbations.

Finally, the inability to guarantee the absence of unbound gauge modes does not necessarily imply that it is impossible to design an evolution scheme that is long-term stable and convergent. As we shall see, by adjusting the standard ADM system with constraint terms, stable evolutions are possible even in the presence of these gauge modes.

VI. STABLE ADJUSTED ADM SYSTEMS IN 1D

We consider next a series of lapse-shift choices. For each choice, we investigate (1) the quasi well-posedness of the resulting system of adjusted ADM evolution equations, (2) the propagation of the constraints and (3) the convergence and stability of numerical simulations.

A. Exact Lapse + Area Locking

We can take advantage of the assumed spherical symmetry of the problem and "lock" the area of constant-r surfaces. That is, we exploit the lapse-shift freedom and set $\partial_t\,g_{\theta\theta} = 0$, or equivalently $\partial_t\,b = 0 \;\forall\; t$. From Eq. (3.10), this yields

$$0 = -\beta\,\partial_r\,b + \alpha\,b\,K_b \;\; , \tag{6.1}$$

which can be seen as an algebraic equation to solve for β or α. We will use (6.1) as

$$\beta = \frac{\alpha\,b\,K_b}{\partial_r\,b} \;\; , \tag{6.2}$$

with b determined by the initial data. In our case, for both iEF and PG coordinates, $b = r$. In addition, we choose an exact lapse, i.e. an arbitrary but *a priori* specified function of spacetime. Here again, since the goal is to reproduce numerically the analytic solution, we set the lapse to that given by the iEF or PG solutions.

This exact lapse, area locking (EL+AL) gauge condition has previously been investigated in Ref. [27]. However, the implementation of locking the area was done at the numerical level. That is, condition (6.2) was not explicitly used. Instead, during the temporal updating of grid functions, a correction to the shift was introduced to keep the area locked. With this numerical area-locking and with blending outer boundary conditions, stable simulations were reported in Ref.. [27] for computational domains with $r_o \leq 11\,m$.

Interestingly enough, this EL+AL choice of lapse and shift yields an ADM system of equations already first order in space and quasi-linear; namely,

$$\partial_t u = A \, \partial_r u + B \, u \tag{6.3}$$

with

$$u = \begin{pmatrix} a \\ K_a \\ K_b \end{pmatrix} \quad \text{and} \quad A = \begin{pmatrix} \beta & 0 & \alpha \, a \, r \\ \dfrac{r \, \partial_r \, \alpha + 2 \, (1 - \mu) \, \alpha}{a^3 \, r} & \beta & 0 \\ \dfrac{\alpha}{a^3 \, r} & 0 & \beta \end{pmatrix} ,$$

where β is given by (6.2) and we have set $b = r$ to simplify notation. In the numerical evolutions, however, we do not set $b = r$. The numerical code includes the evolution equation for b. We do not explicitly write the matrix B since it is not necessary for the analysis below. However, we must emphasize that, in order to achieve stability, a value of $\mu \geq 1$ is in principle needed (see Sec. IV).

Although this EL+AL case is not representative of the general ADM equations, where second spatial derivatives do appear, we will use it to introduce the main techniques and ideas regarding quasi well-posedness. We notice first that the matrix A has eigenvalues

$$\lambda_1 = \beta \tag{6.4}$$

$$\lambda_2 = \beta + \frac{\alpha}{a} \tag{6.5}$$

$$\lambda_3 = \beta - \frac{\alpha}{a} , \tag{6.6}$$

and corresponding eigenvectors

$$\vec{e}_1 = [0, 1, 0] \tag{6.7}$$

$$\vec{e}_2 = \left[a^2 \, r, \frac{r \, \partial_r \, \alpha + 2 \, (1 - \mu) \, \alpha}{\alpha}, 1 \right] \tag{6.8}$$

$$\vec{e}_3 = \left[-a^2 \, r, \frac{r \, \partial_r \, \alpha + 2 \, (1 - \mu) \, \alpha}{\alpha}, 1 \right] . \tag{6.9}$$

Because all of the eigenvalues are real and distinct, the system (6.3) is strictly hyperbolic independent of the addition of the constraint term. The EL+AL system of equations is then an example of a hyperbolic system that, unless suitable constraint-terms are added, is subject to developing rapidly growing solutions (see Ref. [2] for another example). It is also important to notice that λ_1 represents a characteristic speed corresponding to propagation along the timelike normal to the foliation. Similarly, λ_2 and λ_3 are characteristic speeds along the light cone.

Let's now consider the particular case of initial data and lapse function constructed from the single black hole solution in iEF or PG coordinates. The eigenvalues are given in these coordinates by

$$\lambda_1 = \frac{2 \, m}{r + 2 \, m} = \sqrt{\frac{2 \, m}{r}} \tag{6.10}$$

$$\lambda_2 = 1 = \sqrt{\frac{2 \, m}{r}} + 1 \tag{6.11}$$

$$\lambda_3 = \frac{2 \, m - r}{2 \, m + r} = \sqrt{\frac{2 \, m}{r}} - 1 , \tag{6.12}$$

where the first and second equalities are for iEF and PG coordinates, respectively. Since the excision boundary r_e is by construction inside the black hole horizon (i.e. $r_e \leq r_h \equiv 2 \, m$), we have that all the eigenvalues are positive there. By looking at the principal part of Eq. (6.3), it is easy to see that non-negative eigenvalues imply propagation of field variables in the direction of decreasing r-coordinate. Therefore, at r_e all the fields propagate out of the computational domain into the hole singularity, thus boundary conditions are not required. On the other hand, at the outer boundary r_o, one has $\lambda_3 < 0$, with the remaining eigenvalues still non-negative. At r_o, one has then two ingoing modes (λ_1 and λ_2) and only one outgoing (λ_3). Given this information, it is perfectly possible to impose a condition suppressing

modes entering the computational domain. However, as we mentioned before, we choose not to do so and impose at r_o the analytic, exact solutions. The direct consequence will be the appearance of a pulse at the outer boundary of the computational domain due to discontinuities in the truncation errors between the outermost evolved point and the boundary point r_o. This pulse propagates in the direction of the black hole and leaves the computational domain through the excision boundary.

The next step is to analyze the effect that the EL+AL choice has on the propagation of the constraints. At the continuum level, for arbitrary choice of lapse, shift and initial data (g_{ij}, K_{ij}) satisfying the constraints (3.3) and (3.4), the evolution equations (3.1) and (3.2) guarantee, ignoring for the moment boundary conditions, that the evolved data will continue to satisfy the constraints. If one now takes into consideration boundary conditions, it is important to keep in mind that boundary data (g_{ij}, K_{ij}) must satisfy the constraints. By looking at the way the constraints propagate, i.e. their characteristics, one gains insight about the allowed boundary conditions consistent with the constraints. Another important aspect of well-posedness in the propagation of the constraints is that it guarantees that there will be no unbounded high frequency growth appearing in the constraints if they are not exactly satisfied at the initial slice (for example, due to numerical errors). This well-posedness for the constraint propagation is a non-trivial property, not possible to prove for generic formulation of Einstein's equations [29].

What we look for are evolution equations for the constraints, equations that would hold if the system (6.3) is satisfied. They can be found by taking time derivatives in both sides of equations (3.13) and (3.14), replacing the time derivatives of the metric by the r.h.s. of equations (3.9–3.12), and finally expressing the metric and its spatial derivatives in terms of the constraints and their spatial derivatives. Following this procedure, it is not too difficult to show that

$$\partial_t v = P \, \partial_r v + Q \, v \,, \tag{6.13}$$

where now

$$v = \begin{pmatrix} H \\ M \end{pmatrix} \quad \text{and} \quad P = \begin{pmatrix} \beta & \dfrac{4\alpha}{a^2} \\[2ex] \dfrac{\alpha}{4} & \beta \end{pmatrix} . \tag{6.14}$$

The matrix P has eigenvalues $\bar{\lambda}_1 = \lambda_2$, $\bar{\lambda}_2 = \lambda_3$, with λ_2 and λ_3 given by (6.5) and (6.6), respectively. This implies that the system (6.13) is also strictly hyperbolic with characteristic speeds along the light cone. Notice that the constraints at r_e propagate out of the computational domain into the hole singularity, consistent with the outgoing propagation of the field variables at r_e, namely the tilting, into the black hole, of the light cone. At the outer boundary r_o, there is an ingoing mode ($\bar{\lambda}_2 > 0$). Therefore, one has, as expected, to be careful to provide data at r_o consistent with this entering mode. Since we are imposing at the outer boundary the analytic iEF and PG solutions, the data at r_o already satisfy the constraints. However, as mentioned before, choosing the lapse and shift does not completely fix the gauge freedom, thus one still has to be careful handling the gauge modes described in Sec. V.

Figure 1 shows the L_2 norm of the Hamiltonian constraint as a function of time. The initial data is given by the iEF analytic solution (3.21), and the lapse and shift are chosen from the EL+AL conditions. Similar results were obtained with PG coordinates. The computational domain extends from $r_e = 1\,m$ to $r_o = 40\,m$. We tried larger and smaller values for r_o. However, the stability of the simulations was not affected by the location of the outer boundary. We use an upwind parameter $q = 0.5$ and a constraint-term parameter $\mu = 2$. We show runs for resolutions of $\Delta r = m/5$, $m/10$, $m/20$, $m/40$ with $\Delta t = 0.25\,\Delta r$. The run with $\Delta r = m/5$ has a resolution similar to those used in three-dimensional simulations of black hole collisions.

Figure 2 shows the L_2 norm of the Hamiltonian constraint (top) and the L_2 norm of the mass (3.35) error (bottom) taken at time $t = 200\,m$ as a function of resolution. The convergence rate implied by the Hamiltonian constraint is 2.18 and by the mass error 1.7. The convergence rate from the Hamiltonian constraint is larger than second order because we used third order accurate discretizations of the advection term as well as third order accurate extrapolations at the excision. On the other hand, the convergence rate obtained from the mass error is less than second order because the mass function is proportional to g^{rr}, a quantity difficult to handle numerically near the singularity. The reason for using the Hamiltonian constraint and mass to monitor accuracies and convergence is because of the gauge invariant nature of these quantities. Finally for reference, we show in Fig. 3 the L_2 norm of the solution Hamiltonian constraint as a function of time for runs with resolution $\Delta r = m/10$ varying the parameter μ. Different lines correspond to values of $\mu = 0.0$, 0.025, 0.5, and 2 in order of stability improvement. It is clear from this figure the dramatic effect that the added constraint term has on the stability of the simulations.

B. Ingoing Null + Area Locking

The ingoing null + area locking (IN+AL) recipe to specify the lapse and shift consists of, in addition to locking the areal coordinate, imposing the condition that the vector $\partial_t - \partial_r$ remains null throughout the evolution. This null condition is only compatible with the iEF case since by construction the iEF solution is based on ingoing null observers. An analogous (ingoing timelike) condition can be obtained for the PG case. In terms of the spacetime metric, the ingoing null condition is stated as $g_{tt} - 2\,g_{tr} + g_{rr} = 0$, or similarly in terms of 3+1 metric functions in (3.5) as

$$\alpha = a\,(1 - \beta)\,. \tag{6.15}$$

Conditions (6.15) and (6.1) yield

$$\alpha = \frac{a}{arK_b + 1} \quad \text{and} \quad \beta = \frac{arK_b}{arK_b + 1}\,, \tag{6.16}$$

where we have set $b = r$ since by construction b remains locked to r. This prescription for the lapse and shift has been successfully applied in the past [30–32].

In order to make the ADM equations in the IN+AL gauge a first order in space system, we need to introduce two new variables: $w \equiv \partial_r a$ and $y \equiv \partial_r K_b$. Even after this choice is made, there is no unique way of writing the resulting equations as a quasi-linear system. The reason is the ambiguity one encounters when dealing with the terms involving $\partial_r a$. One has the choice to either keep it as $\partial_r a$, substitute it with w, or a combination of both. Either choice changes the principal part of the equation. However, in our case, we need only to find a choice that yields a strongly hyperbolic system. It turns out that the simplest choice of replacing $\partial_r a$ by w everywhere yields a system that is well-posed. That is, the resulting ADM equations have the form

$$\partial_t u = A\,\partial_r u + B\,u\,, \tag{6.17}$$

with

$$u = \begin{pmatrix} a \\ K_a \\ K_b \\ y \\ w \end{pmatrix} \tag{6.18}$$

and

$$A = \frac{1}{z^2} \begin{pmatrix} 0 & 0 & 0 & 0 & 0 \\ 0 & z\,a\,r\,K_b & 0 & r & -a^{-2} \\ 0 & 0 & 0 & 0 & 0 \\ 0 & z\,a\,K_b & 0 & z + a^2 r^2 K_b^2 & a^{-1}\,K_b \\ 0 & -z\,a^2 & 0 & a^2\,r & a\,r\,K_b(1+z) \end{pmatrix}\,, \tag{6.19}$$

where we have introduced $z \equiv 1 + a\,r\,K_b$ to simplify notation. The corresponding eigenvalues and eigenvectors are

$$\lambda_1 = 0 \quad \text{with eigenvectors} \quad \vec{e}_1 = [1, 0, 0, 0, 0] \quad,\quad \vec{e}_2 = [0, 0, 1, 0, 0]\,, \tag{6.20}$$
$$\tag{6.21}$$
$$\lambda_2 = 1 \quad \text{with eigenvectors} \quad \vec{e}_3 = [0, 1, 0, 0, -z\,a^2] \quad,\quad \vec{e}_4 = [0, 0, 0, 1, a^2 r]\,, \tag{6.22}$$
$$\tag{6.23}$$
$$\lambda_3 = \frac{arK_b - 1}{z} \quad \text{with eigenvector} \quad \vec{e}_5 = [0, 1, 0, -aK_b, a^2]\,. \tag{6.24}$$

Notice that all the eigenvectors are independent, and, thus, the system is strongly hyperbolic. Also notice that the eigenvalues λ_2 and λ_3 are again the characteristic speeds $(\beta \pm \alpha/a)$ along the light cone. Furthermore, in iEF

11

coordinates, $\lambda_3 = (2\,m - r)/(2\,m + r)$. Therefore, one encounters a similar situation to that of the EL+AL case; namely, at r_e all the eigenvalues are non-negative, and at r_o one has that only $\lambda_3 < 0$. The existence, uniqueness, and well-posedness for IN+AL follows then as with EL+AL case.

Regarding the constraints, their evolution is also described by a strongly hyperbolic system with characteristic speeds along the light cone. It is important to stress that our ADM equations already imply this, i.e. it does not have any relation to making the evolution equations first order in space. In fact, the principal part of the evolution equations for the constraints is exactly the same as in the EL+AL gauge, but now the lapse and shift are given by (6.16). Thus, the analysis and conclusions also follow as in that case.

An interesting aspect of the IN+AL choice is that it is possible to find the general solution to Einstein's equations. We start by defining $f \equiv r\,a\,K_b$. We then use the momentum constraint (3.14) to eliminate K_a from the other equations. The outcome is that we need only to solve three of the four equations (3.9), (3.11-3.13). We choose to work with the Hamiltonian constraint, (3.13), and Eqs. (3.9) and (3.12). The resulting system of equations reads

$$0 = a\,(f^2 + a^2 - 1) + 2\,r\,a\,f\,\partial_r f + 2\,r\,(1 - f^2)\,\partial_r a \tag{6.25}$$

$$(\partial_t - \partial_r)\,a = \frac{a\,(f^2 + a^2 - 1)}{2r(1 + f)^2} \tag{6.26}$$

$$(\partial_t - \partial_r)\,f = \frac{(f^2 + a^2 - 1)}{r(1 + f)}\,. \tag{6.27}$$

The general solution of these equations is

$$f = \frac{2\,m}{r} - C\left(1 - \frac{2\,m}{r}\right) \tag{6.28}$$

$$a^2 = (1 + C)\,(1 + f) \tag{6.29}$$

where $C = C(t + r)$ and m a constant. In terms of the 3+1 variables, the solutions reads

$$a^2 = (1 + C)(1 + f)\ ,\quad b^2 = r^2\ ,\quad K_a = \partial_r\left(\frac{f}{a}\right)\ ,\quad K_b = \frac{f}{a\,r}\ ,\quad \alpha = \frac{a}{1 + f}\ ,\quad \beta = \frac{f}{1 + f}\,, \tag{6.30}$$

with the line element (3.5) explicitly given by

$$ds^2 = -(1 + C)^2\left(1 - \frac{2\,m}{r}\right)dt^2 + 2\,(1 + C)\left[\frac{2\,m}{r} - \left(1 - \frac{2\,m}{r}\right)C\right]dt\,dr \tag{6.31}$$

$$+ (1 + C)\left[1 + \frac{2\,m}{r} - \left(1 - \frac{2\,m}{r}\right)C\right]dr^2 + r^2\,d\Omega^2\,. \tag{6.32}$$

By setting $C = 0$ one recovers the iEF solution (3.21). Also, it is not difficult to show from the gauge invariant definition of mass (3.35) that the parameter m is indeed the mass of the black hole. An important property of the general solution (6.31) is that it shows explicitly the residual gauge freedom associated with the IN+AL choice of lapse and shift. We have found explicitly the equivalence-class of solutions gauge related to the iEF solutions that satisfy the IN+AL lapse-shift condition.

We repeat the same type of numerical experiment as with the EL+AL case, same parameter values, resolutions, boundary conditions and initial data. The lapse and shift are however constructed in this case from (6.16). Figure 4 shows the L_2 norm of the Hamiltonian constraint as a function of time for different resolutions. Figure 5 shows the L_2 norms of the Hamiltonian constraint (top) and mass error (bottom) for different resolutions. The convergence rate are similar to those in EL+AL, namely 2.19 from the Hamiltonian constraint and 1.7 from the mass error. Finally, Fig. 6 shows the L_2 norm of the Hamiltonian constraint as a function of time for a resolution of $\Delta r = m/10$. Different lines correspond to values of $\mu = 0.0, 0.025, 0.5$, and 2 in order of stability improvement. It is clear from this results that the stability behavior of the system of equations under the IN+AL gauge choice follows closely that of EL+AL.

C. Exact Lapse + Exact Shift

Finally, we consider the case in which the lapse function and shift vector are prescribed by the exact analytic solutions. To date, it has not been possible to obtain with the standard ADM system long-term stable and convergent numerical evolutions under the EL+ES choice. Before we present results of EL+ES evolutions using the adjusted

ADM system of equations, let us investigate its quasi well-posedness properties. To make the evolution equations first order in space, we add a new variable $y = \partial_r b$. Once more, the resulting set of equations have the form

$$\partial_t u = A \, \partial_r u + B \, u \,, \tag{6.33}$$

with

$$u = \begin{pmatrix} a \\ b \\ K_a \\ K_b \\ y \end{pmatrix} \tag{6.34}$$

and

$$A = \begin{pmatrix} \beta & 0 & 0 & 0 & 0 \\ 0 & 0 & 0 & 0 & 0 \\ \dfrac{b \, \partial_r \alpha + 2 \, (1 - \mu) \, \alpha y}{a^3 b} & 0 & \beta & 0 & -\dfrac{2 \, (1 - \mu) \, \alpha}{a^2 b} \\ \dfrac{\alpha y}{b a^3} & 0 & 0 & \beta & -\dfrac{\alpha}{a^2 b} \\ 0 & 0 & 0 & -\alpha b & \beta \end{pmatrix} \,. \tag{6.35}$$

The matrix A has eigenvalues

$$\lambda_1 = \beta \tag{6.36}$$
$$\lambda_2 = \beta \tag{6.37}$$
$$\lambda_3 = 0 \tag{6.38}$$
$$\lambda_4 = \beta + \alpha/a \tag{6.39}$$
$$\lambda_5 = \beta - \alpha/a \,. \tag{6.40}$$

There are two fields that propagate with characteristic speed (β) along the normal to the hypersurfaces in the foliation, one field with zero speed and two other fields with characteristic speeds ($\beta \pm \alpha/a$) along the light cone. It is not difficult to show that the eigenvectors corresponding to the eigenvalue $\lambda_1 = \lambda_2 = \beta$ are not distinct, whatever the value of μ. Therefore, the system of equations is only weakly hyperbolic and thus not quasi well-posed, as we have already seen by considering the EL+ES gauge perturbations by themselves in Sec. V.

As in the previous two cases, the the constraints propagate according to

$$\partial_t v = P \, \partial_r v + Q \, v \,, \tag{6.41}$$

where now

$$v = \begin{pmatrix} H \\ M \end{pmatrix} \tag{6.42}$$

and

$$P = \begin{pmatrix} \beta & \dfrac{4\alpha}{a^2} \\ \dfrac{\alpha}{4} & \beta \end{pmatrix}$$

This is, we have the same situation as before, namely propagation of the constraints along with characteristic speeds along the light cone.

We have carried out the same numerical experiments as for the previous two cases. However, for the iEF solution, the simulations with computational domains for $r_o \geq 40\,m$ crashed. We have been able to identify two possible

13

sources behind this problem. One of them is the pulse originated at the outer boundary due to discontinuities of the truncation error. This pulse propagates in the direction of the black hole (i.e. decreasing r-coordinate) with the characteristic speed β. As the pulse travels its amplitude grows in time. This effect is shown in Fig. 7. Here we plot the solution error for the metric function a as a function of space and time for a resolution $\Delta r = m/10$ and outer boundary located at $r_o = 40\,m$. The simulation stops because this pulse-error increases to the point that the metric function a becomes negative. For small computational domains ($r_o < 40\,m$), the crossing time of this pulse is short enough and does not allow a catastrophic growth of the pulse. The pulse is able to leave the computational domain through the excision boundary without crashing the simulation. Since the initial amplitude of this pulse is $O(\Delta r^2)$, i.e. the accuracy of the discretization, in principle one could find a resolution small enough such that the growth of the pulse does not affect the life of the simulation. However, accessing those fine resolutions in three-dimensional simulations is likely to be impractical. The second, and perhaps more severe, source of the problem is the presence of the zero velocity mode. Zero velocity modes were in principle also allowed in the case of IN+AL, see Eq. (6.20). However, the adjusted IN+AL system yields only numerical solutions of the general form (6.31), which clearly does not contain a zero velocity mode. If $\mu = 0$, these zero velocity modes are not suppressed and eventually terminate the simulation. This catastrophic effect induced by zero velocity modes has been previously noticed by Alcubierre et.al [13].

Figure 8 shows the L_2 norm of the Hamiltonian constraint as a function of time with resolution $\Delta r = m/10$ for different locations of the outer boundary. For computational domains with approximately $r_o \leq 40\,m$, the zero velocity mode is still present, but is damped eventually. The reasons why this mode stops growing remain unclear. Nonetheless, there is a strong indication that this behavior is connected to the particular choice of coordinates used to set the exact lapse and shift. If one, instead of the iEF solution, sets the lapse and shift from the PG solution, the outcome of the simulations is completely different. EL+ES simulations with PG lapse and shift are long term stable and convergent for arbitrary sizes of the computational domain as long as the system of equations was adjusted with $\mu \geq 1$. Figure 9 shows the L_2 norm of the solution error for the metric function a as a function of time for different resolutions with $r_o = 40\,m$ for EL+ES in PG coordinates.

VII. CONCLUSIONS

We have demonstrated that, at least for the case of single black hole spacetimes in spherical symmetry, it is possible to obtain long-term stable and convergent numerical simulations using the standard ADM system of equations if the equations are adjusted by introducing terms involving the constraints. Results were presented for three choices of lapse and shift. In addition, we introduced the concept of quasi well-posedness, which appears to be useful in characterizing the properties of the system of evolution equations. We are currently investigating the extension of this approach to three-dimensional evolutions.

ACKNOWLEDGMENTS

[1] J. York, in *Sources of Gravitational Radiation*, edited by L. Smarr (Cambridge University Press, Cambridge, England, 1979).
[2] M. A. Scheel, T. W. Baumgarte, G. B. Cook, S.L. Shapiro and S.A. Teukolsky, *Phys. Rev. D*, **58**, 044020 (1998).
[3] H. Friedrich, *Proc. Roy. Soc. Lond.*, **A375**, 169 (1981); *Proc. Roy. Soc. Lond.*, **A378**, 401 (1981).
[4] Y. Choquet-Bruhat and J.W. York, *C.R. Acad. Sci. Paris*, **t.321**, Série I, 1089 (1995).
[5] S. Frittelli and O. Reula. *Phys. Rev. Lett*, **76**, 4667, (1996).
[6] C. Bona, J. Masso, E. Seidel and J. Stela, *Phys. Rev. D*, **56**, 3405 (1997).
[7] A. Anderson and J. York, *Phys. Rev. Lett*, **82**, 4384, (1999).
[8] For reviews on hyperbolic methods for Einstein's equations: "The Cauchy problem for the Einstein equations", H. Friedrich and A. Rendall, in *Einstein's Field Equations and their Physical Interpretation*, ed. by B. G. Schmidt, Springer, Berlin,

2000. Published in *Lect. Notes Phys.* **540**, 127 (2000). e-Print Archive: gr-qc/000207. Also: "Hyperbolic methods for Einstein's equations", O. Reula, *Living Reviews in Relativity* (http://www.livingreviews.org)

[9] M. Shibata and T. Nakamura *Phys. Rev. D*, **52**, 5428 (1995).

[10] T. Baumgarte and S. Shapiro. *Phys. Rev. D*, **59**, 024007 (1999).

[11] M. Scheel, private communication (2001).

[12] R. Arnowitt, S. Deser and C.W. Misner, in *Gravitation: An Introduction to Current Research*, edited by L. Witten (John Wiley, New York, 1962), pp. 227-265.

[13] M. Alcubierre G. Allen, B. Bruegman, E. Seidel and W. M. Suen, *Phys. Rev. D*, **62**, 124011 (2000).

[14] M. Alcubierre G. Allen, B. Bruegman, T. Dramlitsch, J. A. Font, P. Papadopoulos, E. Seidel, N. Stergioulas, W. M. Suen, and R. Takahashi, *Phys. Rev. D*, **62**, 044034 (2000).

[15] M. Miller, gr-qc/0008017 (2000).

[16] O. Brodbeck, S. Frittelli, P. Huebner, O. A. Reula *J. Math. Phys.* **40**, 909 (1999).

[17] G. Yoneda and H. Shinkai, gr-qc/0103032 (2001).

[18] B. Gustafsson, H.-O. Kreiss and J. Oliger, *Time Dependent Problems and Difference Methods* (John Wiley & Sons, New York, 1995)

[19] C.A.J. Fletcher, *Computational Techniques for Fluid Dynamics*, V. I, pp. 335 (Springer-Verlag, Berlin 1991).

[20] S.A. Teukolsky *Phys. Rev. D*, **61**, 087501, (2000).

[21] L. Rezzolla, A. Abrahams, R. Matzner, M. Rupright, S. Shapiro, *Phys. Rev. D.*, **59**, 064001 (1999).

[22] M. Alcubierre and B. Bruegman, gr-qc/0008067 (2000).

[23] P. Painlevé, *C. R. Acad. Sci. (Paris)*, **173**, 667 (1921).

[24] A. Gullstrand, *Arkiv. Mat. Astron. Fys.*, **15** (6), 1 (1922).

[25] C. Misner, K. S. Thorne, and J. Wheeler, *Gravitation* (W. H. Freeman and Co., San Francisco, 1973).

[26] K. Martel and E. Poisson, gr-qc/0001069 (2000).

[27] L. Lehner, M. Huq, M. Anderson, E. Bonning, D. Schaefer and R. Matzner, *Phys. Rev. D*, **62**, 044037 (2000).

[28] T. W. Baumgarte, S. A. Hughes and S. L. Shapiro, *Phys. Rev. D*, **60**, 087501 (1999).

[29] S. Frittelli, *Phys. Rev.* **D** 55, 5992 (1997).

[30] R. L. Marsa and M. W. Choptuik, *Phys. Rev. D.*, **54**, 4929, (1996).

[31] J. Thornburgh, gr-qc/9906022 (1999).
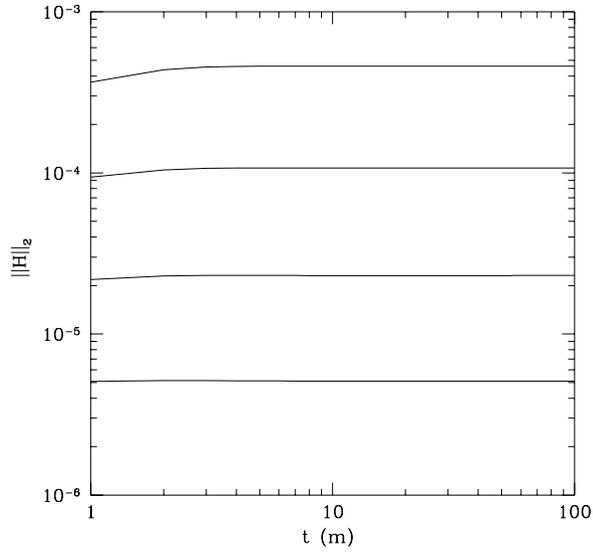
[32] M. Iriondo and O. Reula, gr-qc/0102027 (2001).

FIG. 1. L_2 norm of the Hamiltonian constraint as a function of time for iEF initial data and EL+AL lapse-shift. The computational domain extends from $r_e = 1\,m$ to $r_o = 40\,m$. Lines from top to bottom correspond to resolutions of $\Delta r = m/5$, $m/10$, $m/20$, $m/40$, respectively.
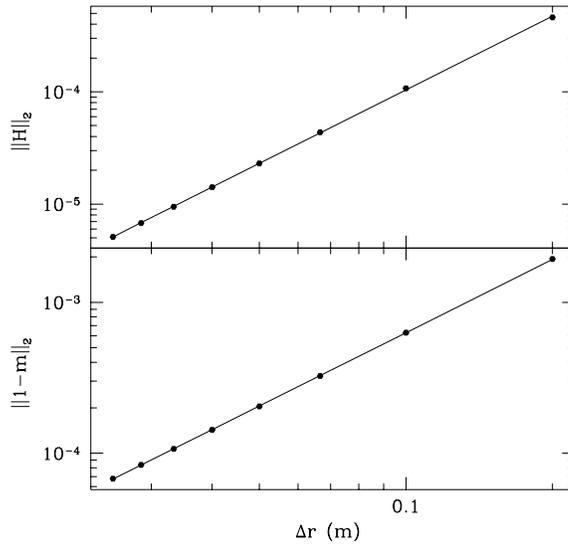

FIG. 2. L_2 norm of the Hamiltonian constraint (top) and L_2 norm of the mass error (bottom) as a function of resolution. The errors plotted were obtained at $t = 200\,m$. The convergence rate implied by the Hamiltonian errors is 2.18 and by the mass error 1.7.
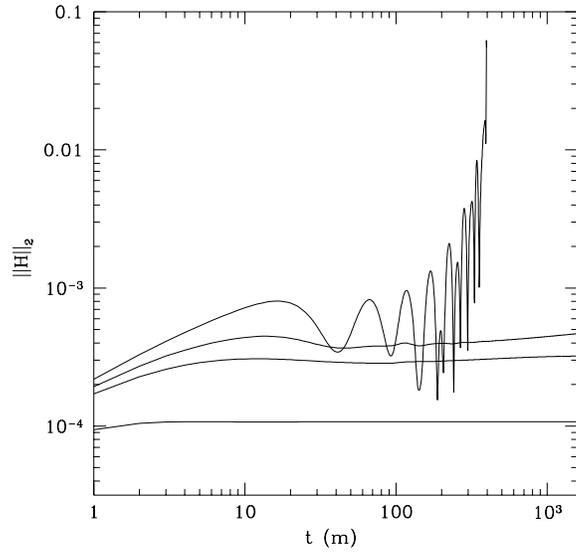
FIG. 3. L_2 norm of the Hamiltonian constraint as a function of time for $\Delta = m/10$ and $r_o = 40\,m$. Each line corresponds to different values of the constraint-term parameter μ. The values of μ are 0.0, 0.025, 0.5 and 2 in order of stability improvement.
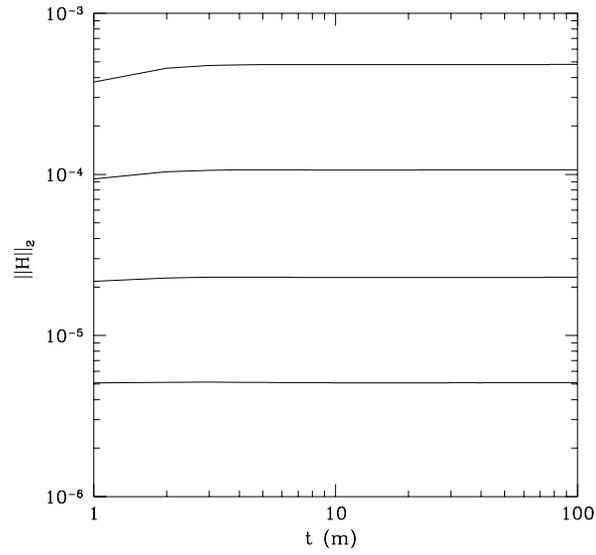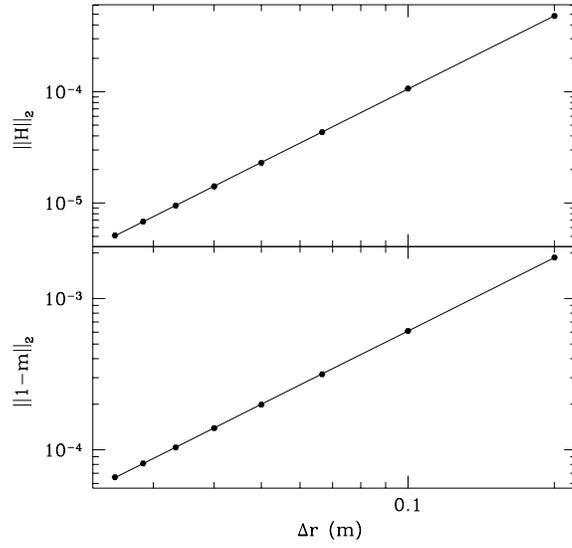

FIG. 4. Same as in Fig.1 but for the IN+AL case.

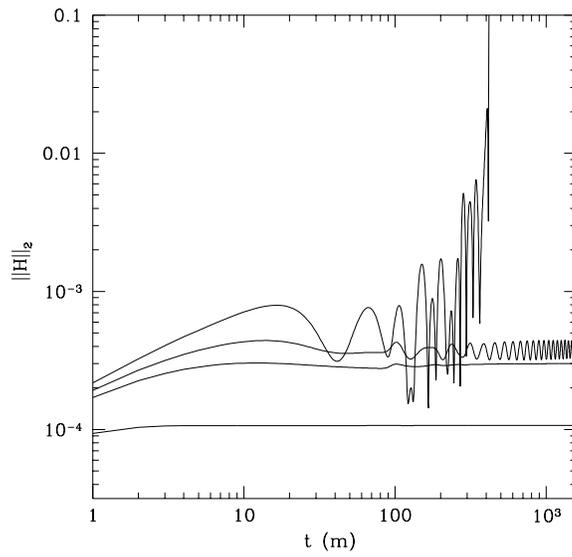FIG. 5.   Same as in Fig.2 but for the IN+AL case.
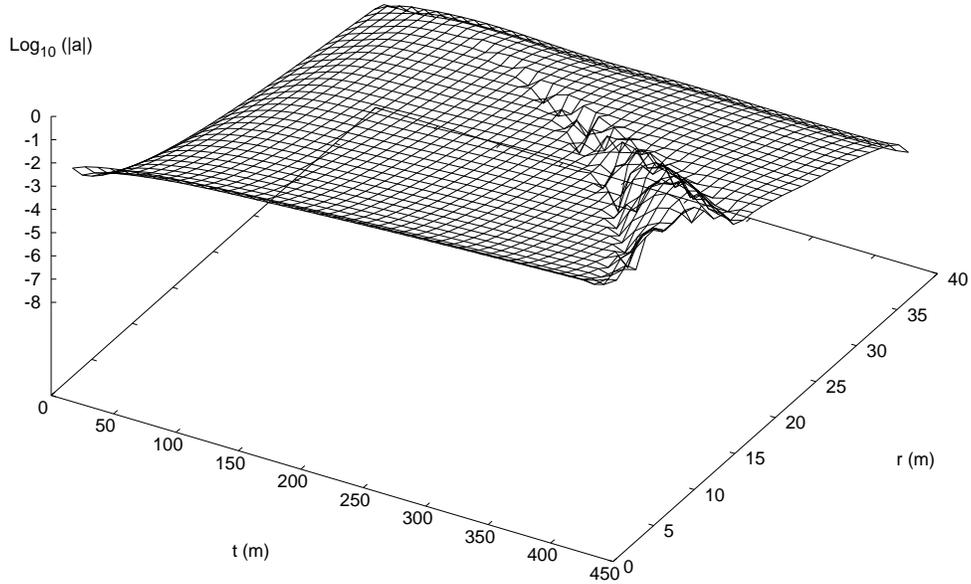

FIG. 6.   Same as in Fig.3 but for the IN+AL case.

18

FIG. 7. Solution error for the metric function a in iEF coordinates for the EL+ES case. The resolution is $\Delta r = m/10$, and the outer boundary is located at $r_o = 40\,m$. A pulse originated at the location of the outer boundary due to discontinuities in the truncation error propagates in the direction of the black hole (decreasing r-coordinate). The simulation stops because this pulse-error increases to the point that the metric function a becomes negative.
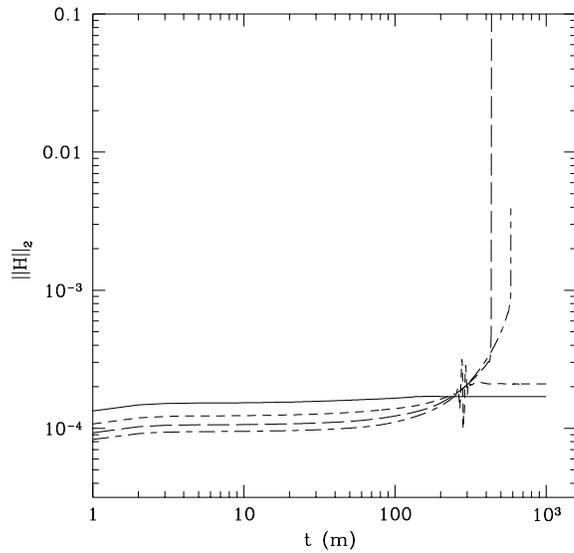

FIG. 8. L_2 norm of the Hamiltonian constraint in iEF coordinates for the EL+ES case as a function of time. The resolution is $\Delta r = m/10$ and $\mu = 2$. Each line corresponds to different location of the outer boundary: $r_o = 20\,m$ (solid), $30\,m$ (short dash), $40\,m$ (long dash), $50\,m$ (short dash long dash).
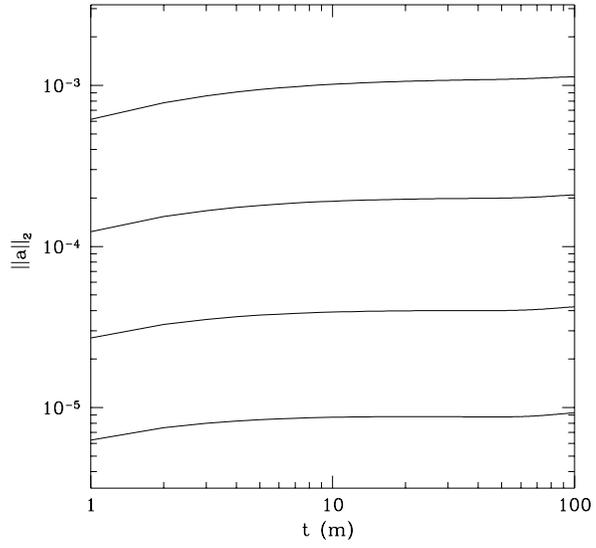
19

FIG. 9. L_2 norm of the solution error in PG coordinates of the metric function a as a function of time. Each line correspond to different resolutions, $\Delta r = m/5$, $m/10$, $m/20$, $m/40$, respectively from top to bottom.